Original Research Paper

Impact of the amount of PEG on prodrug nanoassemblies for efficient cancer therapy

Yaqiao Li [a,1], Lingxiao Li [a,1], Qianhui Jin [a], Tian Liu [a], Jin Sun [a], Yongjun Wang [a], Zhijun Yang [b], Zhonggui He [a,*], Bingjun Sun [a,*]

[a] Wuya College of Innovation, Shenyang Pharmaceutical University, Shenyang 110016, China
[b] School of Chinese Medicine, Hong Kong Baptist University, Hong Kong 999077, China

ARTICLE INFO

ABSTRACT

PEGylation has been widely used to improve the pharmacokinetic properties of prodrug self-assembled nanoparticles (prodrug-SANPs). However, the impacts of the amount of PEG on the self-assemble stability, cellular uptake, pharmacokinetics, and antitumor efficacy of prodrug-SANPs are still unknown. Herein, selenoether bond bridged docetaxel dimeric prodrug was synthesized as the model prodrug. Five prodrug-SANPs were designed by using different mass ratios of prodrugs to PEG ($W_{prodrug}/W_{DSPE-mPEG2000} = 10:0, 9:1, 8:2, 7:3$ and $6:4$), and defined as Pure drug NPs, 9:1NPs, 8:2NPs, 7:3 NPs and 6:4 NPs, respectively. Interestingly, 8:2 NPs formed the most compact nanostructure, thus improving the self-assemble stability and pharmacokinetics behavior. In addition, the difference of these prodrug-SANPs in cellular uptake was investigated, and the influence of PEG on cytotoxicity and antitumor efficacy was also clarified in details. The 8:2 NPs exhibited much better antitumor efficacy than other prodrug-SANPs and even commercial product. Our findings demonstrated the pivotal role of the amount of PEG on prodrug-SANPs.

1. Introduction

Chemotherapy is still the mainstay in the therapy of cancer clinically [1]. However, the clinical application of most chemotherapeutics (such as docetaxel, DTX) is limited by poor delivery efficiency [2]. Many strategies have been used to improve the delivery efficiency of chemotherapeutics including prodrug strategies [3], nanoparticulate drug delivery system (nano-DDS) [4–8]. Prodrug can change the physics and chemistry character of drug such as lack of stability, low solubility and nonselective toxicity by modifying the structure of the parent drug [9]. Due to enhanced permeability and retention (EPR) effect, nano-DDS facilitates the high accumulation of drug in tumor [10]. In addition, prodrug self-assembled nanoparticles (prodrug-SANPs), which inheriting the benefits of prodrug and nano-DDS, have become a hotspot

---

of drug delivery [9]. Since the prodrug is both the carrier and the drug, prodrug-SANPs possess extremely high drug loading and relative low excipient associated side effects [11].

Most nanomedicines, including prodrug-SANPs, generally require hydrophilic materials to modify the surface of the nanoparticles to improve their pharmacokinetic properties [12]. Polyethylene glycol (PEG), a commonly used surface modification material, is one of the few synthetic polymers approved by the FDA [8,13]. PEG is formed by the polymerization of ethylene oxide, and has the advantages of neutral pH, high hydrophilicity [14]. Moreover, PEG possesses the advantages of non-toxicity, non-immunogenicity, and good biocompatibility [15–17]. Modification of prodrug-SANPs with hydrophilic PEG can prevent or minimize the surface adsorption of proteins [18] thus repelling opsonization [19]. Therefore, coating with PEG, a process called PEGylation, can increase the circulating half-life of prodrug-SANPs by avoiding phagocytosis of reticuloendothelial system (RES) [12,20–23]. One example is the first FDA approved anticancer liposome (Doxil®). PEGylation of liposomes using DSPE-PEG$_{2000}$ reduces the phagocytosis of RES, thereby increasing the half-life and circulation time of Doxil® [20–22].

PEG not only affect the systemic circulation time of prodrug-SANPs, but also affect the stability and cellular uptake of prodrug-SANPs [20]. Especially, for prodrug-SANPs, which the main body of the nanostructure is the prodrug molecule [23], the addition of PEG and the amount of PEG are possible to impact the assembly ability and assembly stability of the prodrug, thereby affect its *in vivo* fate. In addition, the modification of hydrophilic PEG can provide a hydration shell on the surface of the prodrug-SANPs, which will impact the cellular uptake of the prodrug-SANPs [24]. Therefore, the amount of PEG materials on prodrug-SANPs demands comprehensive consideration and design, taking into account the stability, cellular uptake and pharmacokinetics behavior of prodrug-SANPs. However, none of the correlational research has been reported to our knowledge.

In this study, we designed the selenoether linker bridged docetaxel dimeric prodrug as a model drug to systematically explore the effect of the amount of PEG on the drug delivery efficiency of the prodrug-SANPs [11,25]. Five prodrug-SANPs were developed by using different ratios of prodrugs to PEG ($W_{prodrug}/W_{DSPE-mPEG2000}$ = 10:0, 9:1, 8:2, 7:3 and 6:4), and defined as Pure drug NPs, 9:1NPs, 8:2NPs, 7:3 NPs and 6:4 NPs, respectively. We clarified the impacts of the amount of PEG on the self-assembly stability, pharmacokinetics, cellular uptake and antitumor efficacy of prodrug-SANPs.

2. Materials and methods

2.1. Materials

DiR, Docetaxel, hydrogen peroxide (H_2O_2), fetal bovine serum (FBS), Trypsin, Dulbecco's modified eagle medium (DMEM, high glucose), Roswell Park Memorial Institute (RPMI-1640) and 3-(4,5-dimethylthiazol-2-yl)−2,5-diphenyltetrazolium bromide (MTT) were bought from Meilun Biotech (Dalian, China). Bromoacetic acid, selenium, 1-ethyl-3-(3-dimethylaminopropyl) carbodiimide hydrochloride (EDCI),

3-bromopropionic acid, sodium borohydride (NaBH$_4$), 4-dimethylaminopyrideine (DMAP), 4-bromobutyric acid were all bought from Aladdin (Shanghai, China). 1,2-distearoyl-sn–glycero-3-phosphoethanolamine-N-methyl (polyethylene glycol)−2000 (DSPE-mPEG$_{2000}$) were obtained from Shanghai Advanced Vehicle Technology Pharmaceutical Ltd. (Shanghai, China). Ki67 cell proliferation kit and TUNEL apoptosis detection kit were obtained from Beijing Solarbio Science & Technology Co., Ltd. Cell culture materials were provided by NEST Biotechnology. All reagents mentioned in this work were of analytical grade.

2.2. Synthesis of selenodiacetic acid linker

The synthesis of selenodiacetic acid linker resembles our previous research [11]. All the reactions were under nitrogen atmosphere. Selenium powder, pure water and NaBH4 solution was mixed. The above mixture was first reacted at 0 °C for 30 min, and then at 105 °C for 1 h. At last, the mixture was added the bromoacetic acid aqueous solution and stirred at 25 °C for 12 h, then removed the impurities from reaction mixture. Using diluted hydrochloric acid regulated pH of the filtrate to 3.0–4.0. Then extracting the product by using ethyl acetate. The precipitation was recrystallized in ethyl acetate and dried to obtain the product selenodiacetic acid [11].

2.3. Synthesis and characterization of dtx dimeric prodrug (DTX-Se-DTX)

DTX and selenodiacetic acid linker was added in CH$_2$Cl$_2$, and used DMAP and EDCI as catalysts for the reaction. Preparative liquid chromatography and Nuclear magnetic resonance spectroscopy (600 MHz ^{1}H NMR, Bruker AV-400) was used to purified and characterized prodrug, respectively. High-resolution mass spectrometry (Agilent 1100 Series LC/MSD Trap) and High Performance Liquid Chromatography (HPLC) were also used in this research.

2.4. Preparation of prodrug-SANPs

2 mg DTX-Se-DTX and 0.22 (9:1), 0.50 (8:2), 0.86 (7:3), 1.33 (6:4) mg DSPE-mPEG$_{2000}$ were well dissolved in 400 μl ethanol. The preparation of different ratios of PEGylated prodrug-SANPs by dropping the mixture ethanol solution into 2 ml deionized water while stirring rapidly. The preparation of non-PEGylated prodrug-SANPs was the same procedure but without adding PEG. Finally, ethanol was removed by using vacuum distillation. All the concentration of prodrug-SANPs were 1 mg/ml. The drug loading of all prodrug-SANPs was calculated as:

$$\text{Drug Loading (\%)} = \text{Weight of DTX} / (\text{Weight of prodrug} + \text{Weight of DSPE} - \text{mPEG}_{2000}) \times 100\%.$$

2.5. Molecular simulations

The molecular dynamics simulations were utilized to illustrate the self-assembly mechanism of PEG and prodrug binding in different proportions. In brief, using Discovery

Studio Client [26] to construct the prodrug molecules and the DSPE-mPEG$_{2000}$ molecules. Quantum mechanics method was used to optimize the small ligand molecule and obtain the stable structure. After the stable configuration was obtained, the Packmol program [27] was used to structure the four prodrug-SANPs. Molecular dynamics simulations were then performed for the complex. The molecular RESP charge [28] parameters were fitted and GAFF field [29] parameters were constructed based on antechamber program in AmberTools [28]. The TIP3P water box model side length is set to 1 nm. Energy minimization was performed at 5000 steps, followed by short-term 100 ps simulation under NVT and NPT ensemble respectively, and finally 30 ns equilibrium simulation was generated. The truncation radius was set at 0.8 nm, the time step was set at 2 fs, and the temperature and pressure were set at 298 K and 1 bar, respectively. The configurations are saved every 10 ps for subsequent analysis. All molecular simulations were calculated by Gromacs2018 program [30]. Combined free-energy calculations are implemented using the g_mmpbsa tool [31].

2.6. Stability of prodrug-SANPs

The four prodrug-SANPs were stored at 4 °C and 25 °C 14 days to test the storage stability [32]. Further, 10% FBS and 90% PBS (pH 7.4) was used to simulate the *in vivo* environment, and investigated the *in vivo* stability of different ratios of PEGylated prodrug-SANPs for 24 h [33]. The interactions between prodrug-prodrug molecules or prodrug-PEG molecules were test by treating four prodrug-SANPs with of urea, SDS or NaCl. All of the above medium were shaken in 37 °C. All the concentration of prodrug-SANPs in above medium were 0.05 mg/ml. At scheduled time points, the diameter was determined ($n = 3$ for each group).

2.7. In vitro drug release

Mixture of 70% PBS (pH 7.4) and 30% ethanol (v/v) was used as release medium to measure the *in vitro* drug release behavior [34]. The different ratios of PEGylated prodrug-SANPs and DTX solution were added in release medium with or without predetermined of H_2O_2 (equivalent DTX concentrations of 6.67 μg/ml). HPLC was applied to determine the peak area of theoretic DTX and DTX released from prodrug-SANPs at the scheduled time ($n = 3$ for each group). Drug release rate (%) = Peak area of released DTX / Peak area of theoretic DTX × 100%. All of the above medium shook at 37 °C. Confirming the intermediate by using LC/MSD.

2.8. Cell culture

Mouse mammary carcinoma cells (4T1 cells), mouse prostate cancer cells (RM-1 cells) and mouse fibroblast cells (3T3 cells) were supplied from the cell bank of Type Culture Collection of Chinese Academy of Sciences. The 4T1 cells were cultured in RPMI-1640 medium. And the RM-1 cells and 3T3 cells were cultured in DMEM medium. All cells grew in cell incubator filled with 37 °C, 5% CO_2.

2.9. Cytotoxicity assays

4T1 cells, RM-1 cells, 3T3 cells were put in 96-well plates for 1000 cells per well and cultured 12 h. The fresh medium was applied for further incubating 48 h which containing with various concentrations of DTX solution or different ratios of PEGylated prodrug-SANPs, and utilized the cells without treatment as control group. MTT was added to all plates and cultured for 4 h and replaced by dimethyl sulfoxide (DMSO). The survival rates were analyzed by using microplate reader and determined the IC$_{50}$ values ($n = 3$ for each group) by Prism 9. The selective index (SI) values were gained from IC$_{50}$ of 3T3 cells to tumor cell lines.

2.10. Cellular uptake

4T1 cells were cultured in 24-well plates (5×10^4 cells per well) for 24 h. Then incubated for 2 h, 4 h and 12 h at 37 °C by using DTX solution and different ratios of PEGylated prodrug-SANPs (equivalent DTX concentrations of 1000 ng/ml and 2000 ng/ml, $n = 3$ for each group). After that, cells were washed thrice by using cold PBS, collected, sonicated and centrifugated. Then, the concentration of free DTX in the cells were measured by UPLC-MS-MS (ACQUITY UPLCTM, Waters Co., Ltd., Milford, MA, USA). Intracellular protein concentration was detected by BCA kit.

2.11. Animal studies

All the animals were provided and approved by the Institutional Animal Ethical Care Committee (IAEC) of Shenyang Pharmaceutical University. The ethics approval number is SYPHU-IACUC–C2021–5–12–106. All experiments about animal were observed the Guidelines for the Care and Use of Laboratory.

2.12. In vivo pharmacokinetic study

Male Sprague–Dawley (SD) rats were used to study the pharmacokinetic profiles of different ratios of PEGylated prodrug-SANPs. The animals were intravenously injected by DTX solution and different ratios of PEGylated prodrug-SANPs (equivalent DTX concentration of 4 mg/kg, $n = 3$ for each group). Plasma was gotten at the predetermined time intervals and analyzed concentrations of prodrugs and free DTX by using UPLC-MS-MS. AUC and C$_{max}$ were calculated using DAS 2.1.1.

2.13. In vivo biodistribution

The tumor model was established by using female BALB/c mice injected by 4T1 cells in the back. When tumor volume reached $\sim$ 400 mm^3, tumor-bearing mice were divided into fifteen groups ($n = 3$ for each group). The mice were injected with DiR solution and DiR-labeled different ratios of PEGylated prodrug-SANPs (equivalent DiR concentrations of 1 mg/kg, equivalent DTX concentrations of 10 mg/kg). The mice of DiR solution and DiR-labeled different ratios of PEGylated prodrug-SANPs were sacrificed at 1 h, 4 h and 12 h. The major

organs including heart, liver, spleen, lung, kidney and tumor of each mouse were isolated for imaging by noninvasive optical imaging system (IVIS). And fluorescence semi-quantitative analysis was performed

2.14. In vivo antitumor efficacy

The tumor model was established by using female BALB/c mice injected by 4T1 cells in the back. The day was regarded as Day 0 for treatment when the tumor size rose to 100 mm^3. Then, the mice were treated with saline, DTX solution and the four different ratios of PEGylated prodrug-SANPs (equivalent DTX concentration of 2 mg/kg, $n = 5$ for each group) every other day for five times. Caliper has been used to measure the maximum diameter (L) and the minimum diameter (W) of the tumor every day. And the body weight was measured daily. The tumor size was calculated as: Tumor (mm^3) $= L \times W \times W \times 0.5$. At the Day 9, the mice were sacrificed, and the tumors and spleens were weighed after treatment. And the tumor burden was calculated by W_{tumor} to W_{mice}. After that, the toxicity of each group was determined. The major organs, and tumor of each group were studied by hematoxylin and eosin (H&E) staining. The lung metastatic nodules were observed after soaking and staining with Bouin's tissue fixative solution. The serum was investigated by hepatic and renal function analysis. TUNEL assay and Ki-67 immunofluorescence staining were investigated to evaluate the apoptosis and proliferation of tumor. DAPI-positive cells were used to observe the processed slides. Image J was used to calculate quantification of the relative area (%) of apoptosis cells and proliferating cells.

2.15. Statistical analysis

GraphPad Prism 7.0 was used to analyze all data. Student's t-test (two-tailed) was used to analyze the statistical comparisons. Statistical significance was considered at *$P < 0.05$, **$P < 0.01$, ***$P < 0.001$ and ****$P < 0.0001$.

3. Results and discussion

3.1. Synthesis of dtx dimeric prodrugs

The synthesis of DTX-Se-DTX was shown in Fig. S1. The chemical structure of the prodrug was confirmed by MS and ^{1}H NMR (Fig. S2). The purity of the prodrug was over 97%.

3.2. Preparation and characterization of prodrug-SANPs

In order to research the influence of DSPE-mPEG$_{2000}$ on the prodrug-SANPs, non-PEGylated prodrug-SANPs and different ratios of PEGylated prodrug-SANPs were prepared (Fig. 2A). According to the different ratios of prodrug to PEG ($W_{prodrug}/W_{DSPE-mPEG2000} = 10:0$, 9:1, 8:2, 7:3, and 6:4), the prodrug-SANPs were defined as Pure drug NPs, 9:1 NPs, 8:2 NPs, 7:3 NPs and 6:4 NPs respectively. As shown in Table S1 and Fig. 2B-F, pure drug could assemble into nanoparticles with a slightly larger diameter of 175.1 nm. 9:1 NPs, 8:2 NPs and 7:3 NPs exhibited similar hydrodynamic diameter around 90 nm.

However, 6:4 NPs showed large and nonuniform particle size (> 300 nm). In addition, Transmission electron microscopy images revealed a uniform spherical morphology of these prodrug-SANPs except 6:4 NPs (Fig. 2B-2F). This indicated that the amount of DSPE-mPEG$_{2000}$ significantly impacted the formation of prodrug-SANPs. Due to the nonuniform particle size, 6:4 NPs was no longer investigated in the follow-up studies. The drug loading capacity of prodrug-SANPs were extremely high even for 7:3 NPs (more than 60%, DTX equivalent, w/w).

3.3. Molecular dynamics simulations of prodrug-SANPs

The molecular dynamics simulations were utilized to elucidate the assembly molecular mechanisms. The conformational variation during molecular dynamics simulations were shown in Fig. 3. As for Pure drug NPs, the conformation of clusters formed loose structure, indicating poor self-assembly ability of Pure drug NPs. In comparison, the conformational variation of PEGylated prodrug-SANPs was formed into stable and tight nanostructure in a relative short time with the hydrophilic PEG facing outward. However, 9:1 NPs and 7:3 NPs formed voids in the middle of the prodrug-SANPs and generated relatively loose nanoparticles. Among three PEGylated prodrug-SANPs, 8:2 NPs assembled into stable nanostructure about 10 ns, demonstrating that 8:2 NPs possessed better self-assembly ability. As for thermodynamics, the binding free energy (ΔG_{total}) and energy decomposition components of Pure drug NPs, 9:1 NPs, 8:2 NPs, 7:3 NPs were calculated and summarized in Table S2. A negative ΔG_{total} indicates favorable system of interactions, and larger absolute values of potential energy expresses better stability. The absolute values of ΔG_{total} of 8:2 NPs (−22,953.60 kJ/mol) was much larger than that of Pure drug NPs (−8948.90 kJ/mol), 9:1 NPs (−10,438.10 kJ/mol), and 7:3 NPs (−18,502.40 kJ/mol). And decomposition components of energy also help to make certain of the contribution of detailed interactions. As expected, van der Waals force was the main force for all the nanoparticles, since the hydrophobic force is the dominant force in self-assembly process (Table S2). Electrostatics, polar energy and non-polar energy also played a leading role in the stability of nanoparticles.

The intermolecular interactions of the prodrug-SANPs were shown in Figure S3A. In addition to the interaction between prodrug molecules, the prodrug also formed hydrogen bond interactions with PEG molecules in the presence of PEG. We also evaluated the radius of gyration and solvent accessible surface of nanoparticles. As shown in Fig. S3B- S3C, the variation of radius of gyration and solvent accessible surface of prodrug-SANPs were followed the order of the 8:2 NPs > 7:3 NPs > 9:1 NPs > Pure drug NPs. The 8:2 NPs, with a maximum change of radius of gyration (about 4 nm) and solvent accessible surface (appropriate 2000 nm^2), formed the most compact nanostructure.

3.4. Stability of prodrug-SANPs

All the prodrug-SANPs were stable with negligible changes in particle size under storage condition (Fig. 4A-4B), during 14 d at 4 °C and 25 °C. The stability of prodrug-SANPs was further
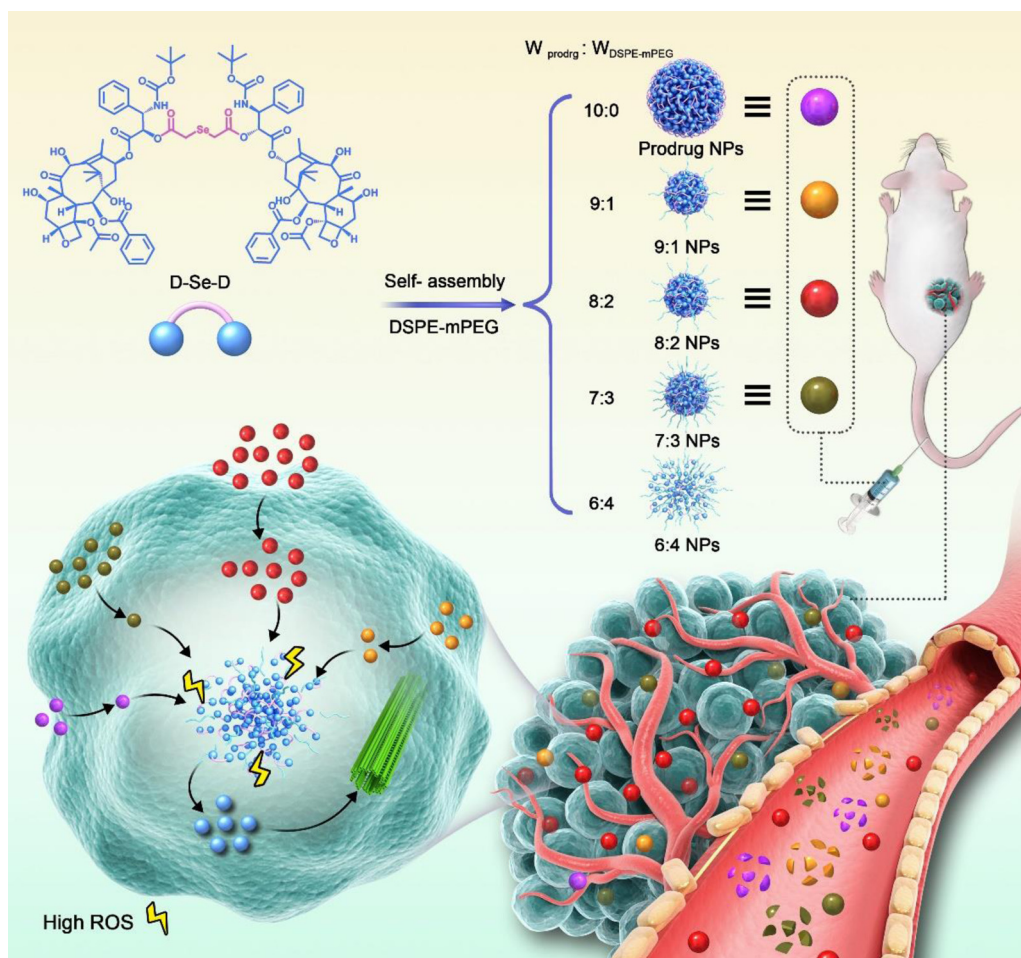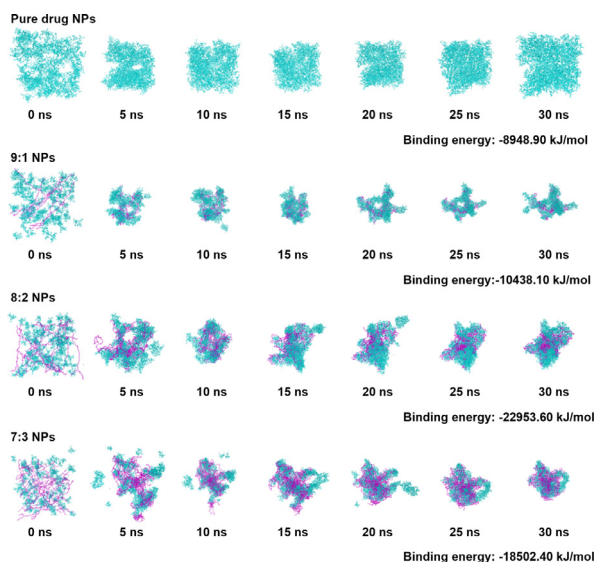
Fig. 1 – Schematic illustration of different ratios of PEGylated prodrug-SANPs for efficient cancer therapy. The ratio of DSPE-mPEG$_{2000}$ significantly impacted the self-assemble stability and cellular uptake of prodrug-SANPs, thereby influencing the *in vivo* fate and antitumor efficacy.
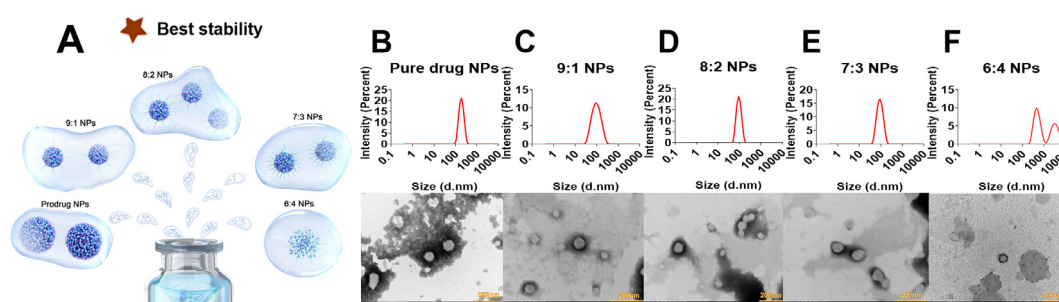
Fig. 2 – Preparation and characterization of prodrug-SANPs. (A) Preparation of different ratios of PEGylated prodrug-SANPs. Particle size distribution and TEM images of (B) Pure drug NPs, (C) 9:1 NPs, (D) 8:2 NPs, (E) 7:3 NPs and (F) 6:4 NPs.

investigated in PBS (pH 7.4) including 10% FBS (v/v) to predict the stability of prodrug-SANPs in the body. Among these four prodrug-SANPs, 8:2 NPs showed excellent stability with insignificant change in particle size even after 24 h (Fig. 4C). In contrast, the particle size of Pure drug NPs, 9:1 NPs and 7:3 NPs were increased in different degrees followed the order of Pure drug NPs > 9:1 NPs > 7:3 NPs. In addition, prodrug-SANPs were treated in NaCl, urea or sodium dodecyl sulfate (SDS),

which could eliminate electrostatic force, hydrogen bonds, and hydrophobic force, respectively. As shown in Fig. 4D-4F, all the prodrug-SANPs were sensitive to SDS rather than urea. This indicated that hydrophobic force is the dominate force in self-assembly, which was in line with the molecular dynamics simulations results (Table S2). Interestingly, the particle size of Pure drug NPs and 9:1 NPs were increased significantly when incubated with NaCl. This finding suggested that Pure drug

Pure drug NPs

0 ns   5 ns   10 ns   15 ns   20 ns   25 ns   30 ns

Binding energy: -8948.90 kJ/mol

9:1 NPs

0 ns   5 ns   10 ns   15 ns   20 ns   25 ns   30 ns

Binding energy:-10438.10 kJ/mol

8:2 NPs

0 ns   5 ns   10 ns   15 ns   20 ns   25 ns   30 ns

Binding energy: -22953.60 kJ/mol

7:3 NPs

0 ns   5 ns   10 ns   15 ns   20 ns   25 ns   30 ns

Binding energy: -18502.40 kJ/mol

Fig 3 – Molecular dynamics simulations of different ratios of PEGylated prodrug-SANPs. Schematic diagram of the aggregation process of prodrug-SANPs from 0 ns to 30 ns (DTX-Se-DTX as shown as blue, and DSPE-mPEG$_{2000}$ as purple).

NPs and 9:1 NPs tended to instability under extreme condition. Both molecular dynamics simulations and stability tests indicated that the amount of PEG impacted the stability of prodrug-SANPs. Moderate DSPE-mPEG$_{2000}$ (8:2) could improve the stability prodrug-SANPs while excess (7:3) or inadequate

DSPE-mPEG$_{2000}$ (9:1 or 10:0) could disturb the self-assemble process. In summary, when the mass ratio of prodrug to PEG was 8:2, the most compact and stable prodrug-SANPs were formed.

3.5. *In vitro drug release*

In blank media, 9:1 NPs, 8:2 NPs and 7:3 NPs exhibited similar release profile, and could release approximately 20% DTX after 24 h. The proportion of DTX released from Pure drug NPs could reach 40% at 24 h (Fig. 5B). These finding demonstrated that the addition of PEG could improve the stability of prodrug-SANPs, thus prevent premature drug release in the blood circulation. In addition, we further explored the oxidation-responsivity of prodrug-SANPs using hydrogen peroxide (H_2O_2) as model triggers. At low H_2O_2 concentration, the drug release from 9:1 NPs, 8:2 NPs and 7:3 NPs were comparable, while the DTX release of Pure drug NPs were slight faster than PEGylated prodrug-SANPs, which were consist with the results in the blank media (Fig. 5C). At high H_2O_2 concentration, all prodrug-SANPs possessed similar drug release rate, and could release 80% DTX after 24 h incorporation (Fig. 5D). DTX-Se-DTX prodrug was the main body of these nanoparticles, and the release of DTX mainly depended on the oxidation of selenoether bond, thereby these prodrug-SANPs exhibited comparable release rate under the high H_2O_2 concentration. The H_2O_2-triggerd drug released mechanism was illustrated in Fig. 5A. The oxidation-responsive selenium atoms were oxidized to hydrophilic selenoxide by H_2O_2, then promoting the hydrolysis of DTX-adjacent ester bond. We next texted the molecular weights of intermediates after oxidation to verify
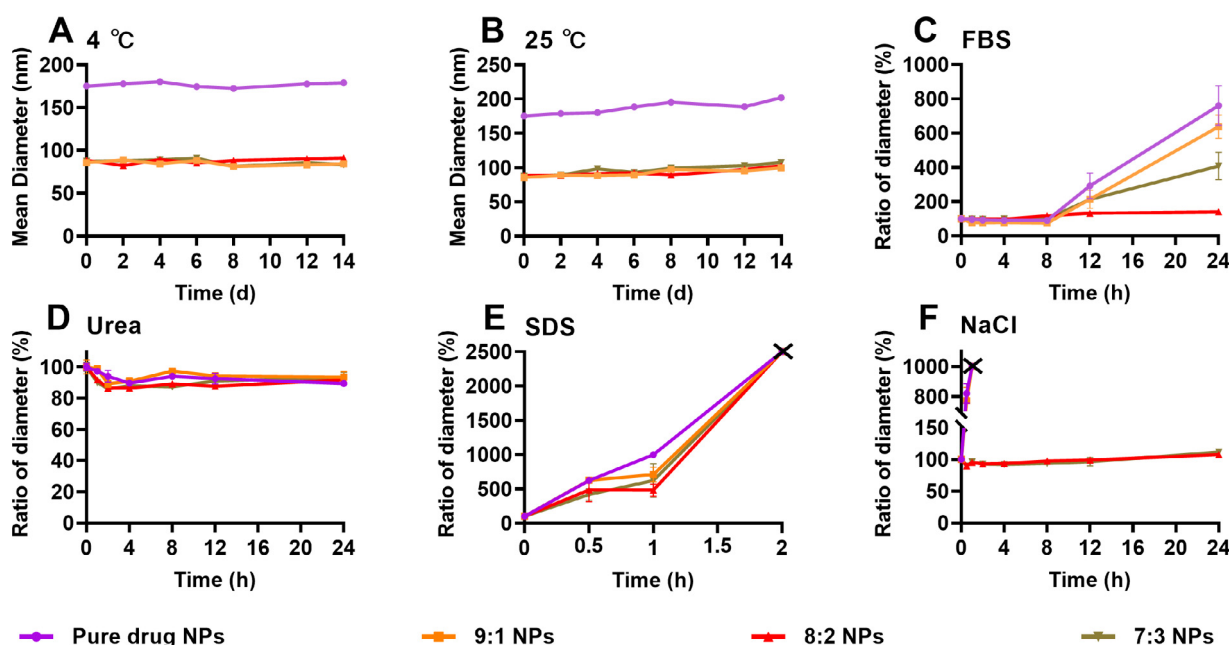
Fig. 4 – Stability of prodrug-SANPs in different environments. Store at 4 °C (A) and 25 °C (B) for 14 d (C) The colloidal stability of prodrug-SANPs in PBS (pH 7.4) including 10% FBS (v/v). Size change curves of prodrug-SANPs incubated with (D) Urea, (E) SDS and (F) NaCl at 37 °C (medium concentration: 0.4 M). Data are presented as mean ± SD (*n* = 3).
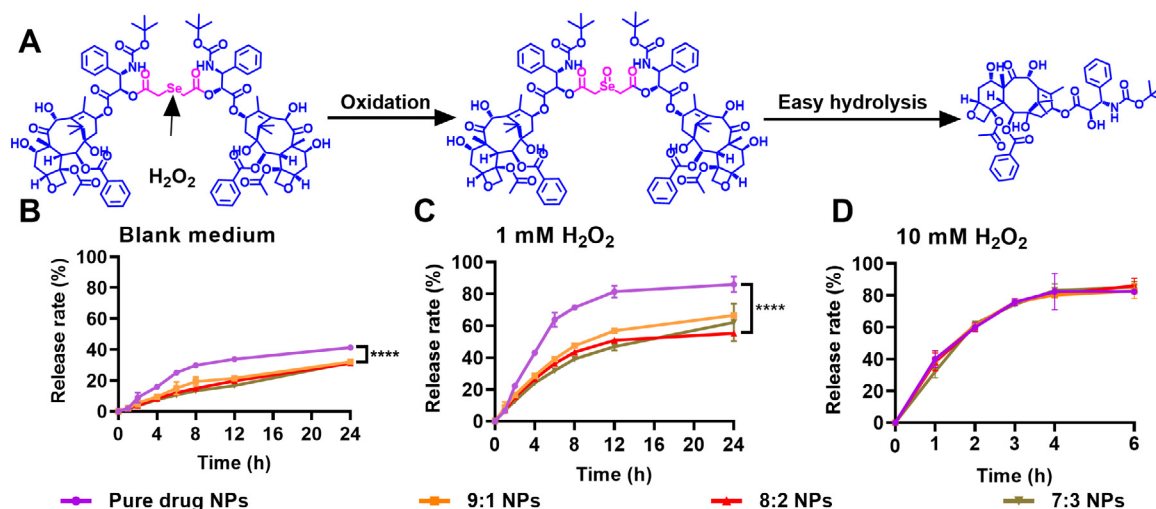
Fig. 5 – *In vitro* drug release of prodrug-SANPs. *In vitro* drug release of prodrug-SANPs in (B) blank medium. Oxidation-responsive drug release of prodrug-SANPs in the presence of (C) 1 mM H_2O_2 and (D) 10 mM H_2O_2. Data are presented as mean ± SD ($n = 3$). **** $P < 0.0001$ by two-tailed Student's t-test.

the mechanism. The molecular weights of the monoxides of DTX-Se-DTX and the released DTX were showed in Fig. S4.

3.6. Cytotoxicity and cellular uptake

The cytotoxicity assay of prodrug-SANPs was conducted in two tumor cells and one normal cell. As shown in Fig. 6A-6B, Fig. S5A- S5B and Table S3, prodrug-SANPs had weaker cytotoxicity than DTX solution in two kinds of tumor cells, following the order of DTX solution ≈ 8:2 NPs > 9:1 NPs > Pure drug NPs > 7:3 NPs. Abovementioned *in vitro* release studies indicated that there was no significant different in these prodrug-SANPs except for Pure drug NPs. Therefore, we speculated that the ratios of PEG modification affected the cellular uptake efficiency of prodrug-SANPs [35], thereby causing the difference of cytotoxicity [36]. The cellular uptake of prodrug-SANPs was further determined in 4T1 cells using UPLC-MS/MS. As shown in Fig. 6D-6E. At 2 h, the cellular uptake of DTX by 8:2 NPs-treated group was significantly higher than that of other prodrug-SANPs and comparable to that of DTX solution. The cellular uptake of these prodrug-SANPs followed the order of DTX solution ≈ 8:2 NPs > 9:1 NPs > Pure drug NPs > 7:3 NPs, which was consistent with the cytotoxicity results. The reason for the high uptake efficiency of DTX solution was that DTX is a lipophilic small molecule drug, which is easy to enter cells through lipophilic cell membrane. Moreover, there are two factors that determine the uptake efficiency of prodrug-SANPs. One is the stability of the prodrug-SANPs, and the other is the amount of PEG on prodrug-SANPs. Pure drug NPs exhibited the poor stability, thereby tended to premature aggregation outside the cells, which limited the efficiency of cellular uptake. Too much modification of PEG on 7:3 NPs not only impacted the stability but also hindered the cellular uptake of prodrug-SANPs. Therefore, 7:3 NPs possessed the poorest cellular uptake efficiency and cytotoxicity. 8:2 NPs formed the most compact and stable prodrug-SANPs, with suitable PEG

modification, showing the highest cellular uptake efficiency and the strongest cytotoxicity, which was comparable to DTX solution (Fig. 6F).

As shown in Fig. 6C & S5C and Table S3, all prodrug-SANPs showed lower cytotoxicity than DTX solution on 3T3 normal cells. To compared the cytotoxicity of prodrug-SANPs and DTX solution between tumor cells and normal cells, we next calculated the selectivity index (SI) and displayed in Table S4. The Pure drug NPs, 9:1 NPs, 8:2 NPs and 7:3 NPs displayed much higher SI values than DTX solution. These results indicated that prodrug-SANPs could selectively kill tumor cells due to oxidation-responsivity release of DTX in response to high oxidation state in tumor cells. in comparison, prodrug-SANPs exhibited negligible DTX released in the normal cells, showing good safety.

3.7. In vivo pharmacokinetics and biodistribution

We next used SD rats to investigate the pharmacokinetic profiles of DTX solution and prodrug-SANPs [37]. The pharmacokinetic profiles were shown in Fig. 7 and Table S5. As expected, DTX in DTX solution and Pure drug NPs were cleared quickly in the blood, while the PEGylated prodrug-SANPs increased the area under the curve (AUC) to different degrees. The AUC of total DTX (released DTX plus DTX in prodrug) in the Pure drug NPs, 9:1 NPs, 8:2 NPs and 7:3 NPs groups were approximately 1.31-, 2.94-, 19.66- and 8.79- times higher than DTX solution group (Table S5). These findings shown that the ratio of DSPE-mPEG$_{2000}$ PEGylated prodrug-SANPs significantly impacted the pharmacokinetic profiles. Among four prodrug-SANPs, the 8:2 NPs, which enhanced colloidal stability, exhibited the highest AUC.

We next determined the biodistribution of prodrug-SANPs in 4T1 tumor-bearing BALB/C mice by using IVIS spectrum (Fig. 8). The results of tumor accumulation were well confirmed to the stability and pharmacokinetic behavior. 8:2 NPs, with the best stability and pharmacokinetic behavior,
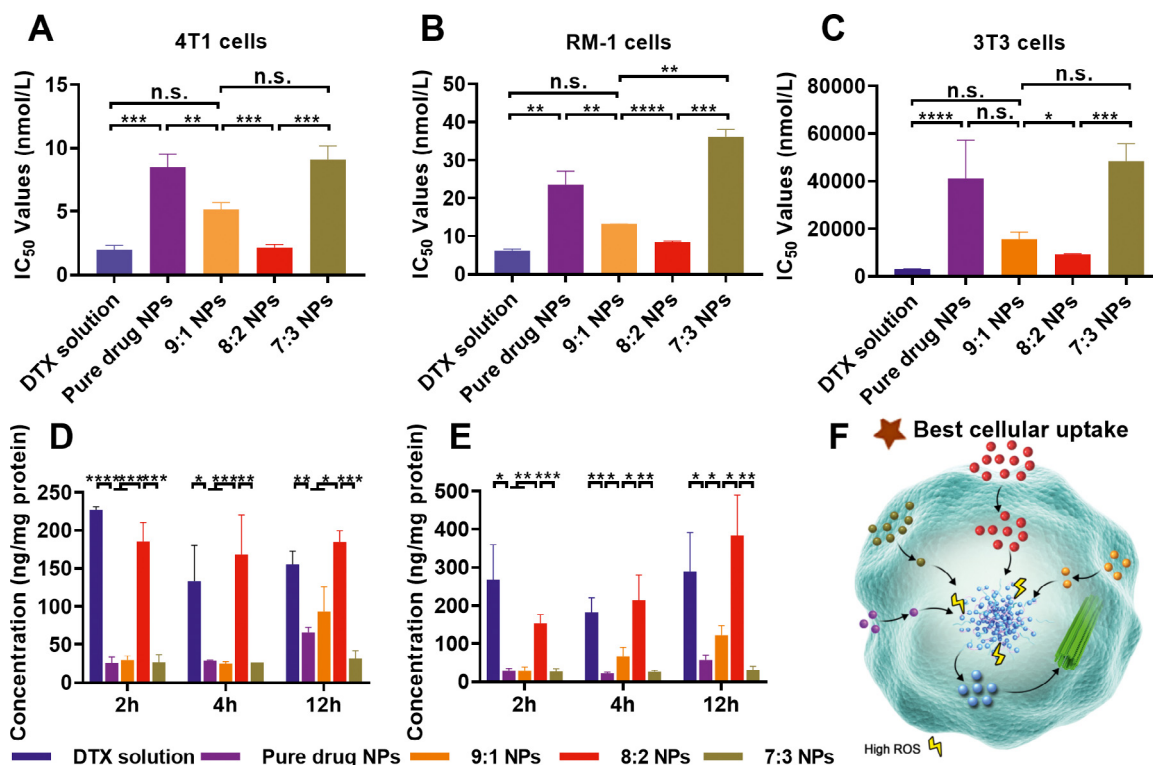
Fig. 6 – IC$_{50}$ values (nmol/L) and cellular uptake of DTX solution and prodrug-SANPs. IC$_{50}$ values (nmol/L) on (A) 4T1 cells, (B) RM-1 cells, (C) 3T3 cells. The cellular uptake of DTX solution and prodrug-SANPs in 4T1 cells at equivalent DTX concentration of (D) 1000 ng/ml and (E) 2000 ng/ml. (F) The cellular uptake efficiency of prodrug-SANPs in tumor cells. Data are presented as mean ± SD ($n = 3$). *$P < 0.05$, **$P < 0.01$, *** $P < 0.001$ and ****$P < 0.0001$ by two-tailed Student's t-test.
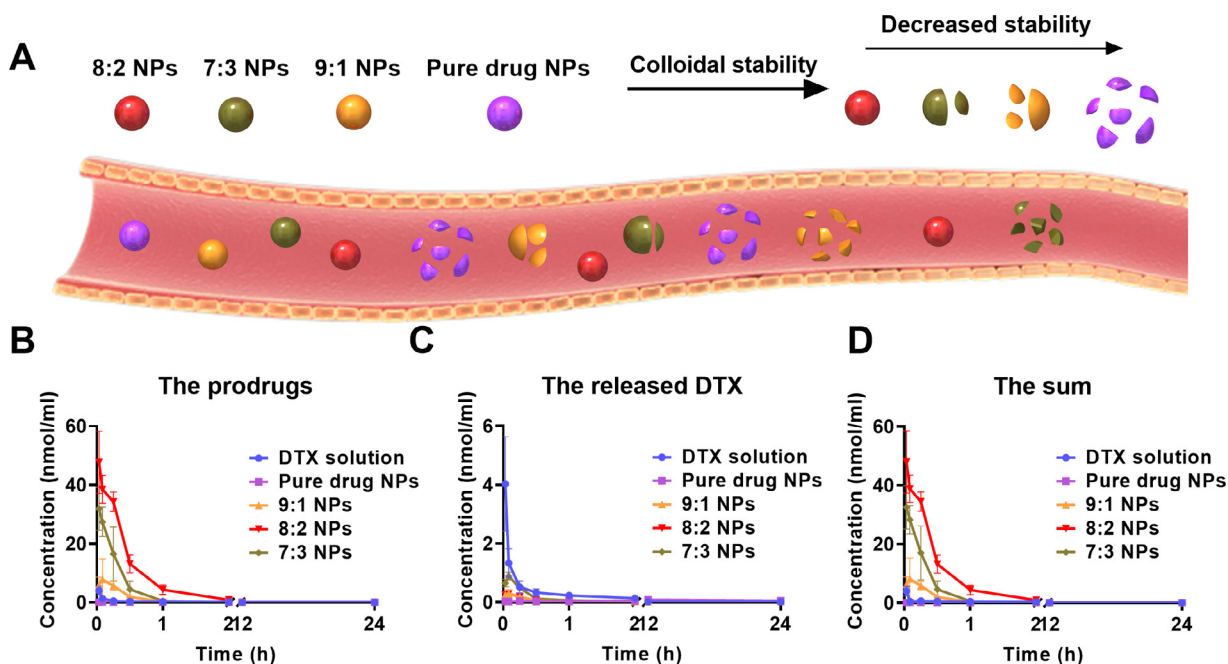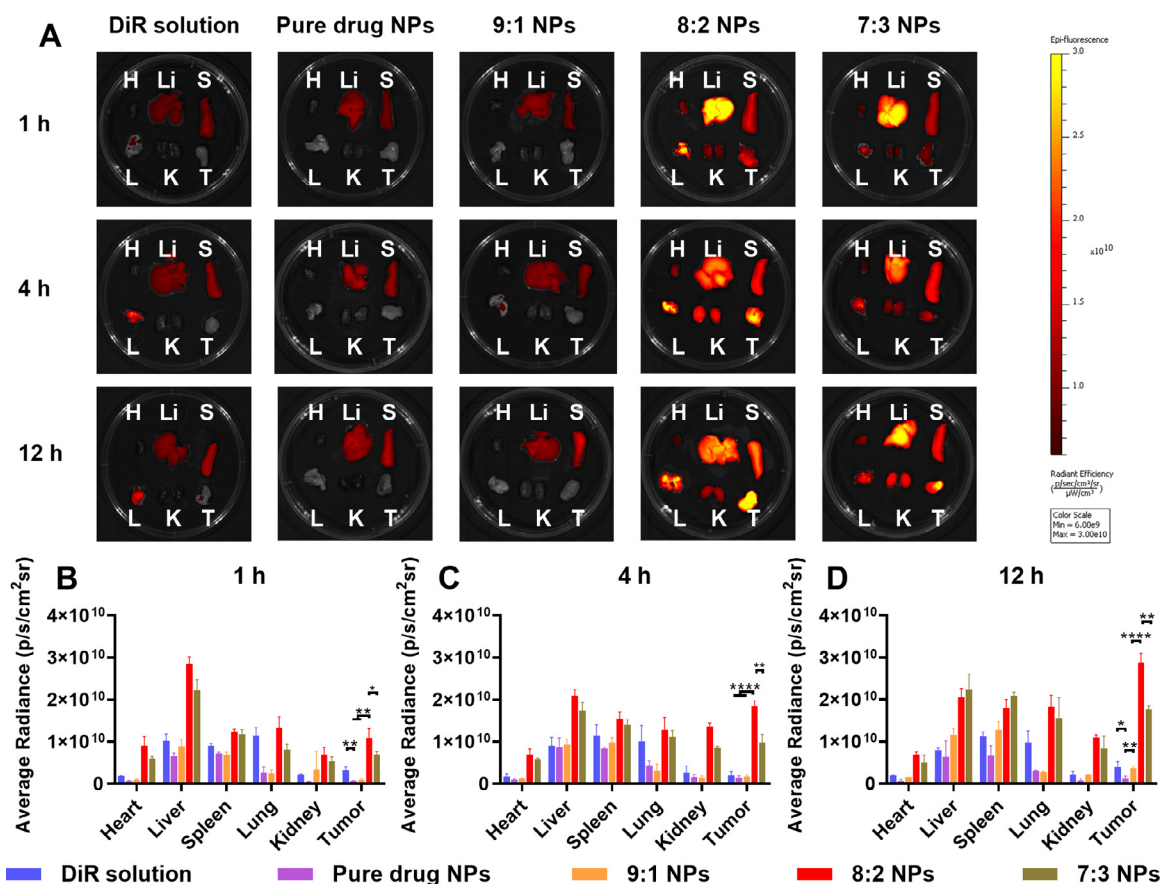

Fig 7 – Pharmacokinetics of PEGylated prodrug-SANPs. (A) Blood circulation affects stability of prodrug-SANPs. Molar concentration–time curves of (B) the prodrugs, (C) the released DTX, and (D) the sum of prodrugs and the released DTX. Data are presented as mean ± SD ($n = 3$).

Fig 8 – Biodistribution of PEGylated prodrug-SANPs. (A) Fluorescent imaging at 1 h, 4 h, 12 h. Fluorescence semi-quantitative analysis of each main organ and tumor at 1 h (B), 4 h (C) and 12 h (D). *$P < 0.05$, **$P < 0.01$ and ****$P < 0.0001$ by two-tailed Student's t-test. Data are presented as mean ± SD (n = 3).

showed the highest accumulation in tumors. The fluorescence of 8:2 NPs in tumor gradually increased from 1 h to 12 h (Fig. 8B-8D). In comparison, DiR solution was mainly concentrated in liver, spleen and lung, and there was almost no fluorescence in tumor. As we expect, Pure drug NPs and 9:1 NPs also showed almost no distribution in tumor. It's possible due to the poor colloid stability of Pure drug NPs and 9:1 NPs, which were cleared quickly in the blood. The 8:2 NPs exhibited significantly better tumor accumulation, which also suggested that the 8:2 NPs has the best antitumor efficacy.

3.8. In vivo antitumor efficacy

We further determined the antitumor activity of DTX solution and prodrug-SANPs (Fig. 9A). On Day 9, the volume of some tumors in the saline group have already reached nearly 1500 mm^3, which would not meet the ethical standards and animal welfare. Therefore, we could not conduct a longer in vivo anti-tumor investigation (Fig. 9B). As shown in Fig. 9B-9D, the Pure drug NPs showed poor antitumor activity due to their poor stability and pharmacokinetic behavior. The antitumor activity of DTX solution was between that of 9:1 NPs and 7:3 NPs groups. In addition, 8:2 NPs exhibited the best antitumor

efficacy, since it possessed the optimal colloidal stability, cytotoxicity, and AUC among these four prodrug-SANPs. We further detected the lung metastasis of 4T1 tumor-bearing mice after five times treatment for each group (Fig. 9E). The visible metastasis sites were circled in white. Among them, 8:2 NPs treated group showed less lung metastasis nodules, and had good anti-metastasis ability. TUNEL assay and Ki-67 assay were used to investigate the cellular apoptosis and the cellular proliferation of tumor tissues (Fig. S6). 8:2 NPs showed significant higher apoptosis and lower proliferation than other groups (Fig. S6C- S6D). TUNEL assay and Ki-67 assay also indicating that 8:2 NPs had the best antitumor efficacy than other groups. Hence, small changes in the ratio of DSPE-mPEG$_{2000}$ for PEGylated prodrug-SANPs have great influences on the antitumor efficacy.

In addition, we investigated the toxicity of DTX solution and the PEGylated prodrug-SANPs by measuring body weight, hepatorenal function, H&E staining, and spleen size in mice. The body weight of mice injected DTX solution showed significant decline, while there was no change in other mice injected prodrug-SANPs (Fig. 9F). The AST values of DTX solution group were abnormal high than saline group or any other groups (Fig. S7), which indicated impaired of hepatic function. As shown in Fig. S8, the lung metastasis in H&E
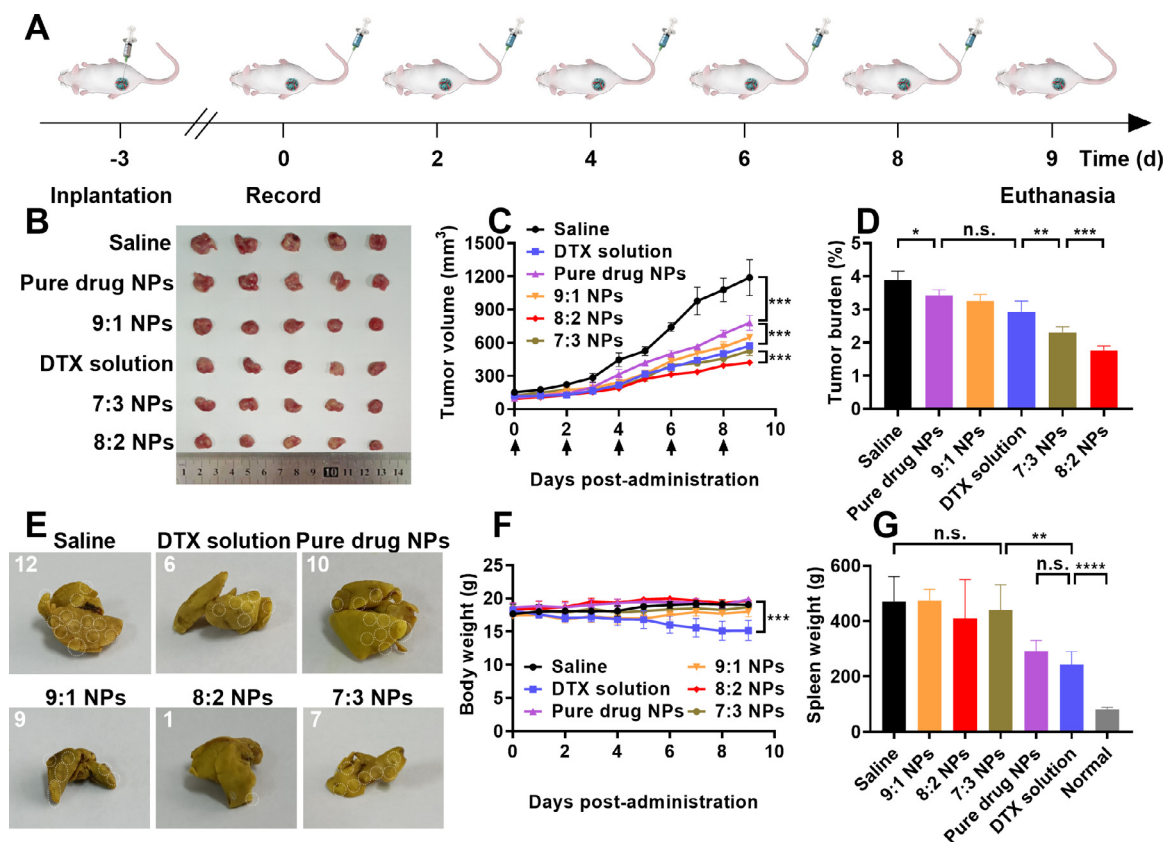
Fig. 9 – The antitumor efficacy of DTX solution and prodrug-SANPs against 4T1 xenograft tumors. (A) Schematic of *in vivo* tumor treatment. (B) Images of tumors. (C) The variation of tumor volume. (D) Tumor burden. (E) Images of lung metastasis. (F) The variation of body weight. (G) Spleen weight. Data are presented as mean ± SD ($n = 5$). *$P < 0.05$, **$P < 0.01$, ***$P < 0.001$ and ****$P < 0.0001$ by two-tailed Student's t-test.

staining was found in all groups, while 8:2 NPs treated group showed fewer lung metastasis nodules. Besides, the spleen of DTX solution and Pure drug NPs treated group was shrunk (Fig. 9G). 4T1 tumor acts in an endocrine fashion to stimulate myelopoiesis with the production and export of large numbers of granulocytes. The rapidly evolving granulocytosis would cause splenomegaly by massive granulocytic infiltrates [38]. Therefore, the spleens and granulocytes of our tumor model groups were all much larger than normal. Some research show that spleen weight is positively correlated with numbers of granulocytes in 4T1 tumor-bearing mice [39]. The granulocytes of DTX solution and Pure drug NPs were significantly lower than other groups (Fig. S9) which was consistent with the trend of spleen weight. The low granulocytes indicated that DTX solution and Pure drug NPs could cause myelosuppression [40].

4. Conclusion

To investigate the influence of the amount of PEG on the self-assembly ability and drug delivery efficiency of prodrug-SANPs, a new oxidation sensitive DTX dimeric prodrug was co-assembled with different ratios of PEG ($W_{prodrug}/W_{DSPE-mPEG2000} = 10:0$, 9:1, 8:2, and 7:3). We found that the amount of PEGylation significantly impacted the

stability of prodrug-SANPs. When the mass ratio of prodrug to PEG was 8:2, the most compact and stable prodrug-SANPs were formed. In addition, 8:2 NPs possessed efficient cellular uptake efficiency and strong cytotoxic activity, which were comparable to DTX solution. The ratios of PEG also significantly impacted the *in vivo* fate of prodrug-SANPs. The 8:2 NPs exhibited higher AUC and much better antitumor efficacy than other prodrug-SANPs and even commercial product. Our findings demonstrated the pivotal role of the amount of PEG on prodrug-SANPs.

Conflicts of interest

The authors report no conflicts of interest. The authors alone are responsible for the content and writing of this article.

Acknowledgments

Supplementary materials

Supplementary material associated with this article can be found, in the online version, at doi:10.1016/j.ajps.2022.02.002.

REFERENCES

[1] Cao W, Zeng X, Liu G, Li Z, Zeng X, Wang L, et al. Porphine functionalized nanoparticles of star-shaped poly (ε-caprolactone)-bd-α-tocopheryl polyethylene glycol 1000 succinate biodegradable copolymer for chemophotodynamic therapy on cervical cancer. Acta Biomater 2015;26:145–58.

[2] Pronk LC, Stoter G, Verweij J. Docetaxel (taxotere): single agent activity, development of combination treatment and reducing side-effects. Cancer Treat Rev 1995;21(5):463–78.

[3] Cheetham AG, Chakroun RW, Ma W, Cui H. Self-assembling prodrugs. Chem Soc Rev 2017;46(21):6638–63.

[4] Mi Y, LiuY Feng SS. Formulation of docetaxel by folic acid-conjugated D-α-tocopheryl polyethylene glycol succinate 2000 (Vitamin E $TPGs_{2k}$) micelles for targeted and synergistic chemotherapy. Biomaterials 2011; 32(16):4058–66.

[5] Gao W, Xiang B, Meng TT, Liu F, Qi XR. Chemotherapeutic drug delivery to cancer cells using a combination of folate targeting and tumor microenvironment-sensitive polypeptides. Biomaterials 2013;34(16):4137–49.

[6] Han HK, Amidon GL. Targeted prodrug design to optimize drug delivery. AAPS Pharm Sci 2000;2(1):48–58.

[7] Sun Q, Zhou Z, Qiu N, Shen Y. Rational design of cancer nanomedicine: nanoproperty integration and synchronization. Adv Mater 2017;29(14):1606628.

[8] Kozma G, Shimizu T, Ishida T, Szebeni J. Anti-PEG antibodies: properties, formation and role in adverse immune reactions to PEGylated nano-biopharmaceuticals. Adv Drug Deliv Rev 2020;154:163–75.

[9] Li L, Zuo S, Dong F, Liu T, Gao Y, Yang Y, et al. Small changes in the length of diselenide bond-containing linkages exert great influences on the antitumor activity of docetaxel homodimeric prodrug nanoassemblies. Asian J Pharm Sci 2021;16(3):337–49.

[10] Zuo S, Sun B, Yang Y, Zhou S, Zhang Y, Guo M, et al. Probing the superiority of diselenium bond on docetaxel dimeric prodrug nanoassemblies: small roles taking big responsibilities. Small 2020;16(45):2005039.

[11] Sun B, Luo C, Zhang X, Guo M, Sun M, Yu H, et al. Probing the impact of sulfur/selenium/carbon linkages on prodrug nanoassemblies for cancer therapy. Nat Commun 2019;10(1):1–10.

[12] Owens DE III, NA Peppas. Opsonization, biodistribution, and pharmacokinetics of polymeric nanoparticles. Int J Pharmaceut 2006;307(1):93–102.

[13] Dawidczyk CM, Kim C, Park JH, Russell LM, Lee KH, Pomper MG, et al. State-of-the-art in design rules for drug delivery platforms: lessons learned from FDA-approved nanomedicines. J Control Release 2014;187:133–44.

[14] Herzberger J, Niederer K, Pohlit H, Seiwert J, Worm M, Wurm FR, et al. Polymerization of ethylene oxide, propylene oxide, and other alkylene oxides: synthesis, novel polymer architectures, and bioconjugation. Chem Rev 2016;116(4) 2170-43.

[15] Sun T, Zhang YS, Pang B, Hyun DC, Yang M, Xia Y. Engineered nanoparticles for drug delivery in cancer therapy. Angew Chem Int Ed 2014;53(46):12320–64.

[16] Sun B, Luo C, Yu H, Zhang X, Chen Q, Yang W, et al. Disulfide bond-driven oxidation- and reduction-responsive prodrug nanoassemblies for cancer therapy. Nano Lett 2018;18(6):3643–50.

[17] Sun BJ, Luo C, Cui W, Sun J, He ZG. Chemotherapy agent-unsaturated fatty acid prodrugs and prodrug-nanoplatforms for cancer chemotherapy. J Control Release 2017;264:145–59.

[18] Moghimi SM, Hunter AC, Murray JC. Long-circulating and target-specific nanoparticles: theory to practice. Pharmacol Rev 2001;53(2) 283-18.

[19] Pillai G. Nanomedicines for cancer therapy: an update of fda approved and those under various stages of development. Soj pharm pharm sci 2014;13.

[20] Behzadi S, Serpooshan V, Tao W, Hamaly MA, Alkawareek MY, Dreaden EC, et al. Cellular uptake of nanoparticles: journey inside the cell. Chem Soc Rev 2017;46(14):4218–44.

[21] Pozzi D, Colapicchioni V, Caracciolo G, Piovesana S, Capriotti AL, Palchetti S, et al. Effect of polyethyleneglycol (PEG) chain length on the bio–nano-interactions between PEGylated lipid nanoparticles and biological fluids: from nanostructure to uptake in cancer cells. Nanoscale 2014;6(5):2782–92.

[22] Michel R, Pasche S, Textor M, Castner DG. Influence of PEG architecture on protein adsorption and conformation. Langmuir 2005;21(26):12327–32.

[23] Moghimi SM, Szebeni J. Stealth liposomes and long circulating nanoparticles: critical issues in pharmacokinetics, opsonization and protein-binding properties. Prog Lipid Res 2003;42(6):463–78.

[24] Barenholz YC. Doxil®—The first FDA-approved nano-drug: lessons learned. J Control Release 2012;160(2):117–34.

[25] Zhang H. Onivyde for the therapy of multiple solid tumors. OncoTargets Ther 2016;9:3001.

[26] Kanth BK, Liou K, Sohng JK. Homology modeling, binding site identification and docking in flavone hydroxylase CYP105P2 in Streptomyces peucetius ATCC 27952. Comput Biol Chem 2010;34(4):226–31.

[27] Martínez L, Andrade R, Birgin EG, Martínez JM. PACKMOL: a package for building initial configurations for molecular dynamics simulations. J Comput Chem 2009; 30(13):2157–64.

[28] Case DA, Cheatham TE III, T Darden, H Gohlke, R Luo, Merz KM Jr, et al. The Amber biomolecular simulation programs. J Comput Chem 2005;26(16):1668–88.

[29] Sprenger KG, Jaeger VW, Pfaendtner J. The general AMBER force field (GAFF) can accurately predict thermodynamic and transport properties of many ionic liquids. J Phys Chem 2015;119(18):5882–95.

[30] Van Der Spoel D, Lindahl E, Hess B, Groenhof G, Mark AE, Berendsen HJC. GROMACS: fast, flexible, and free. J Comput Chem 2005;26(16):1701–18.

[31] Kumari R, Kumar R. Open Source Drug Discovery Consortium, Lynn A. g_mmpbsa • A GROMACS tool for high-throughput MM-PBSA calculations. J Chem Inf Model 2014;54(7):1951–62.

[32] Yang YX, Sun BJ, Zuo SY, Li XM, Zhou S, Li LX, et al. Trisulfide bond–mediated doxorubicin dimeric prodrug nanoassemblies with high drug loading, high self-assembly stability, and high tumor selectivity. Sci Adv 2020;6(45):eabc1725.

[33] Sun M, Deng J, Tang Z, Wu J, Li D, Chen H, et al. A correlation study of protein adsorption and cell behaviors on substrates with different densities of PEG chains. Colloids Surf B 2014;122:134–42.

[34] Luo C, Sun B, Wang C, Zhang X, Chen Y, Chen Q, et al. Self-facilitated ROS-responsive nanoassembly of heterotypic dimer for synergistic chemo-photodynamic therapy. J Control Release 2019;302:79–89.

[35] Papi M, Caputo D, Palmieri V, Coppola R, Palchetti S, Bugli F, et al. Clinically approved PEGylated nanoparticles are covered by a protein corona that boosts the uptake by cancer cells. Nanoscale 2017;9(29):10327–34.

[36] Li G, Sun B, Zheng S, Xu L, Tao W, Zhao D, et al. Zwitterion-driven shape program of prodrug nanoassemblies with high stability, high tumor accumulation, and high antitumor activity. Adv Healthc Mater 2021;10(23):2101407.

[37] Zhao ZQ, Zhang XB, Zhang HY, Shan XZ, Bai MY, Wang Z, et al. Elaborately engineering a self-indicating dual-drug nanoassembly for site-specific photothermal-potentiated thrombus penetration and thrombolysis. Adv Sci 2021:2104264.

[38] Hocking W, Goodman J, Golde D. Granulocytosis associated with tumor cell production of colony-stimulating activity. Blood 1983;61:600–3.

[39] DuPre' SA, Hunter KW Jr. Murine mammary carcinoma 4T1 induces a leukemoid reaction with splenomegaly: association with tumor-derived growth factors. Exp Mol Pathol 2007;82(1):12–24.

[40] Antman KS, Griffin JD, Elias A, Socinski MA, Ryan L, Cannistra SA, et al. Effect of recombinant human granulocyte-macrophage colony-stimulating factor on chemotherapy-induced myelosuppression. N Engl J Med 1988;319(10):593–8.